ACTA PHYSICA SINICA
Volume 2, Number 4 (Overseas Edition) April, 1993

STUDIES ON THE RELATIONSHIPS BETWEEN THE STRUCTURE AND THE LOCALIZED ENERGY STATES OF POLY (ETHYLENE TEREPHTHALATE) ELECTRETS*

ZHANG XING-YUAN (张兴元)
Department of Materials Science and Engineering, University of Science and Technology of China, Hefei 230026, China
ZHOU YI-QIN (周漪琴)
Department of Chemistry, Qingdao University, Qingdao 266071, China

(Received 18 May 1992)

A series of poly(ethylene terephthalate) (PET) films with different degrees of planar orientation [$\Delta(xy)z$], crystallinity (X_c) and molecular weights were prepared by drawing biaxially, annealing at 110 ℃ and γ-irradiation of 0.5–4 MGy. The peaks of localized energy states were separated from the detrapping current curves by means of poling temperature scanning method of thermally stimulated current. The depth of localized energy levels enlarged with the rise of $\Delta(xy)z$, X_c and γ-irradiation dose. The kinds of structural defects increased because of the changes of orientation structure of chains, crystalline structure and molecular chain structure, which caused the number of localized states to increase from 2 to 6 and the distribution width of the depth of localized levels to broaden.

PACC: 6140; 7155J; 8140R

I. INTRODUCTION

In organic solids including polymers, there are a lot of localized energy states (trap levels) in the energy gap between the valence band and the conduction band arisen from structural defects such as crystallite defects, crystalline-noncrystalline boundaries and impurities. The charge carriers can be trapped at these defects, leading to charge storage, thus affects the transport process of charge carriers. Poly (ethylene terephthalate) (PET), referred to as a semicrystalline polymer, consists of both crystalline and noncrystalline (amorphous) regions. Various kinds of localized states of PET produced by the complex supermolecular structure may act as trapping centers for charge carriers, giving a dense distribution of localized levels within the forbidden band[1]. The mean depth of trap levels can be determined by the investigation of the detrapping current peaks (ρ-peaks) of thermally stimulated current (TSC) of electrets[2], yet ρ-peak is a superposition of detrapping currents of different localized states (discrete trapping levels) because their distributions are close together.

By separating the detrapping current curves of different localized states from TSC

* Project supported by the National Natural Science Foundation of China.

spectra, we can reveal the relationships between the supermolecular structure and the localized states, and can further study the various factors affecting the transport process of charge carriers. However, there appear only a few reports dealing with this subject. In the present work, various PET samples with different supermolecular structure are prepared by drawing biaxially, annealing and irradiating with a large dose of γ-rays. The relationships among the structure and the number of localized states as well as the depth of localized levels are investigated.

II. EXPERIMENTAL

Amorphous PET films with a thickness of 500 μm were homogeneous confirmed by X-ray study. The films were processed as follows: (1) drawing biaxially on a drawing equipment at 95 °C so that thermal effects on conformational transition can be avoided; (2) annealing at 110 °C for various time intervals; and (3) irradiating by ^{60}Co γ-rays at room temperature in a dose rate of 8 kGy/h. In this way, a series of PET films with different degrees of planar orientation, crystallinity and molecular weights were obtained.

The degree of planar orientation of the drawn films was measured by the polarized Abbe refracting instrument. It could be characterized by[3, 4]

$$\Delta(xy)z = (n_x + n_y)/2 - n_z, \tag{1}$$

where n_x, n_y and n_z represent respectively the refractive indices in the directions of three coordinate axes. The crystallinity (X_c) of annealed PET was determined by means of the density gradient technique (CCl_4 and 1, 4-dimethyl benzene, 25 °C). The number-average molecular weight ($\overline{M}_n$) of γ-irradiated films was obtained with gel permeation chromatography (Type waters-150C) analysis (solvent: *o*-chlorophenic acid, eluting agent: chloroform), in which the fractional standard models of PET was taken as contrast. The basic parameters of the three kinds of samples are given in Table 1.

Table 1. Structural and technological parameters of PET samples.

Orientation				Crystallization		γ-irradiation		
Sample code	Drawing procedure	Stretch ratio	$\Delta(xy)z$ ($\times 10^{-2}$)	Sample code	X_c (%)	Sample code	Irradiation dose (MGy)	$\overline{M}_n$ ($\times 10^3$)
B-1	biaxial	3×2	1.40	C-1	1.5	R-1	0.51	4.46
B-2	stretching	3×3	2.15	C-2	5.5	R-2	1.21	4.45
B-3	(in sequence)	3×4	6.44	C-3	6.8	R-3	2.05	4.08
B-4		3×5	7.90	C-4	13.7	R-4	3.01	3.13
BS-1	biaxial stretching			C-5	19.8	R-5	4.02	2.66
	(simultaneous in x, y)			C-6	22.5			
		3×3	1.02	C-7	28.7			
T-1	three steps ($x \times y \times x$)			C-8	31.2			
		2.5×3×1.5	4.81					
AMOR		1×1	0		0		0	6.58

Wide-angle X-ray diffraction spectra of the samples were obtained using a Rigaku

automatic diffractometer (Type D/max-r/A) with Ni filtered Cu$K\alpha$ radiations. The investigations of Fourier transform infrared photoacoustic spectroscopy (FTIR/PAS) were carried out by means of a model 170SX FTIR spectrometer and a type JDV-1 photoacoustic detector with a resolution of 4 cm^{-1} in the nitrogen atmosphere at a scanning speed of moving mirror of 0.2498 cm/s for 1500 times of scanning. Absorption spectra of ultraviolet and visible light of γ-irradiated samples were determined with a UV-240 spectrophotometer, an amorphous film being taken as contrast.

Al was deposited under 10^{-8} atm on both sides of each specimen which were used as electrodes. TSC spectra were measured on the apparatus of thermal electrical analyzer manufactured by Toyo Seiki Co. Ltd., Japan, whose sensitivity was 10^{-12} A and input impedance was greater than $10^{12}\,\Omega$. The polarizing time (t_p) was 20 min, the polarizing field intensity (E_p) was 100 kV/cm for oriented samples and 50 kV/cm for annealed and irradiated ones. The detrapping current peaks of the localized states of the specimens were separated in a temperature step of 5 °C.

III. RESULTS AND DISCUSSION

A. Number of localized states and the depth of localized levels

First, we measure the conventional TSC spectra of all specimens listed in Table 1 above room temperature at different heating rates. Figure 1 shows the temperature spectra of sample C-5 at three heating rates and samples B-2, B-4 at a heating rate of 5 °C/min. As regards the sample B-4 with a higher degree of planar orientation (B-3,

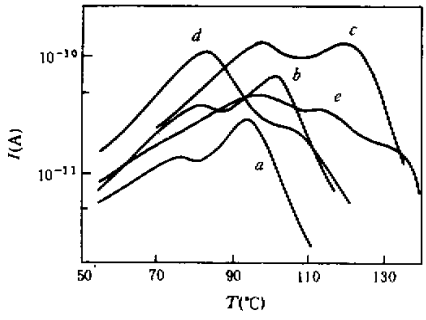

Fig. 1. Temperature spectra of thermally stimulated current of PET samples at the heating rate of *a*: 2 °C/min; b, d, e: 5 °C/min and *c*: 15 °C/min; *a*, *b*, *c*: C-5; *d*: B-2; *e*: B-4.

T-1 are similar), α-peak (attributed to the thermo-relaxation of frozen-in dipoles of segments), ρ-peak (ascribed to the detrapping of trapped charge carriers), and τ-peak (contributed by the detrapping of charge carriers trapped in a deeper trap level)[5] appear

successively from low- to high-temperature regions. With the rise of the heating rate, the current increases, the three peaks shift towards the higher temperature region respectively. As for the oriented samples with lower $\Delta(xy)z$ such as B-1 and B-2, crystallized and γ-irradiated ones, only α- and ρ-peaks are observed, which also shift to the higher temperature regions as the heating rate rises (e.g. C-5 in Fig. 1).

After cleaning up α-peak with the peak cleaning technique of TSC[6], we can obtain the complete detrapping current ρ-peak (including τ-peak if it exists). The temperature regions of detrapping of trapped charge carriers at a certain heating rate can be determined based on ρ-peaks. Within this region, we measured the detrapping current peaks of localized states of samples by means of the poling temperature scanning method[7, 8] under the condition of temperature step $\Delta T=5\,^{\circ}C$. The ρ-peak and detrapping current peaks of localized states of specimen C-6 are shown in Fig. 2. Evidently, the ρ-peak are contributed by the detrapping curves of four localized states. The results of measurement for all samples are listed in Table 2. The ρ-peak of noncrystalline sample consists of the detrapping curves of two localized states. With the rise of $\Delta(xy)z$ and the complication of stretching ways and with the increase of crystallinity and irradiation dose, the number of localized states increases gradually, reaches six at most (sample T-1).

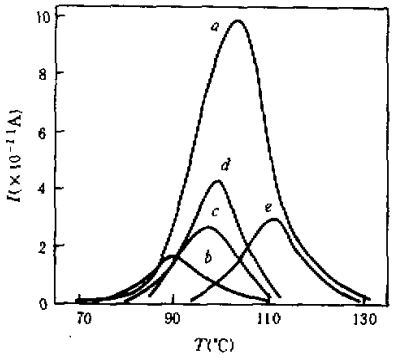

Fig. 2. ρ-peak(a) and detrapping current curves of localized states ($b-e$) of specimen C-6, $\beta=5\,^{\circ}C/min$.

According to the following semiempirical equation proposed by Simmons *et al.* based on the theory of high field[9]

$$\Delta E=T_m[1.92\times10^{-4}\ \log(s/\beta)+0.32\times10^{-3}]-0.0155, \qquad (2)$$

we can calculate the mean depth of localized energy levels ΔE after measuring the detrapping current curves at two or more heating rates (here we take $\beta_1=0.5\,^{\circ}C/min$, $\beta_2=15\,^{\circ}C/min$), where T_m is the temperature of current peak at which the maximum current appears, β is the heating rate, $s\,(=v\sigma_n N_c)$, the frequency factor, is a product of the

Table 2. The localized energy states of PET electrets.

Sample code	No. of localized states	Depth of localized levels (eV) ΔE_i						$\overline{\Delta E_i}$
AMOR	2	1.17	1.22					1.20
BS-1	3	1.84	1.86	1.88				1.86
B-1	4	1.31	1.35	1.38	1.40			1.36
B-2	4	1.32	1.35	1.38	1.42			1.37
B-3	5	1.87	1.89	1.91	1.98	2.02		1.93
B-4	5	2.06	2.10	2.14	2.21	2.24		2.15
T-1	6	1.82	1.85	1.86	1.90	1.92	1.94	1.88
C-1	2	1.18	1.21					1.20
C-2	2	1.28	1.30					1.29
C-3	3	1.29	1.30	1.32				1.30
C-4	3	1.31	1.33	1.36				1.33
C-5	4	1.33	1.36	1.38	1.41			1.37
C-6	4	1.35	1.36	1.38	1.40			1.37
C-7	4	1.36	1.38	1.41	1.44			1.40
C-8	4	1.36	1.38	1.42	1.47			1.41
R-1	3	1.29	1.33	1.36				1.33
R-2	3	1.35	1.39	1.40				1.38
R-3	3	1.47	1.49	1.51				1.49
R-4	3	1.53	1.56	1.57				1.55
R-5	4	1.65	1.66	1.68	1.69			1.67

thermal velocity of an electron, the capture cross section and the effective density of states. Therefrom, we can also calculate the depth of each localized level ΔE_i. ΔE_i and its average value $\overline{\Delta E_i}$ are shown in Table 2.

It can be seen from Table 2 that the depth of localized levels distributes in a certain range. The relationships between the depth of localized levels and the degree of planar orientation, γ-irradiation dose(D) and crystallinity are shown in Fig. 3. The mean depth

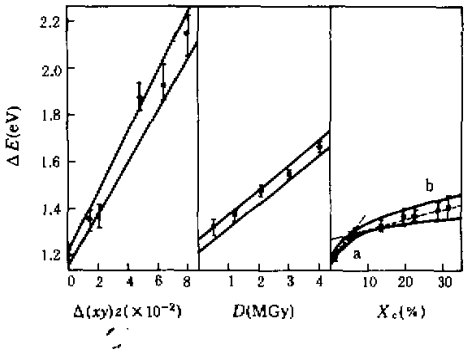

Fig. 3. Correlation of the depth and its distribution width of localized levels with the degree of planar orientation, γ-irradiation dose and crystallinity.

of localized levels increases linearly as $\Delta(xy)z$ and D rise. For the annealed sample, though the average depth still increases with the rise of X_c, the linear relation exhibits a twist at X_c, approximately equal to 5 %. When $X_c < 5$ %, ΔE rises rapidly with X_c(stage *a*), as $X_c > 5$ %, the rise of ΔE becomes slow (stage *b*).

Figure 3 also presents the distribution range of the localized levels. For the oriented and annealed samples, the distribution width increases with $\Delta(xy)z$ and X_c. While in regard to the γ-irradiated ones, the depth of localized levels distributes only within a range of width about 0.06 eV.

B. Relation between the localized states and the structure

No heterogeneous structure was found for amorphous samples by X-ray diffraction. However, it is obvious that the surface and bulk of materials possess different ability for storage and transport of charge carriers. Introducing the concepts of surface trap (surface localized states) and bulk trap (bulk localized states)[8], we may consider that the two localized states of amorphous PET correspond to the surface and bulk localized states respectively.

When the samples are drawn three times as large simultaneously in *x*- and *y*-direction, the number of localized states increases from two (sample AMOR) to three; when stretched biaxially in sequence, the number rises gradually to five, as presented in the series of B-1 to B-4 of Table 2. The larger the enlargement in drawing is, the greater the number of localized states will be. Moreover, the number increases to six due to the three steps stretching in *x*-, *y*- and *x*-direction. If an amorphous PET is drawn, the molecular chains of random arrangement will oriente in the stretching direction (*x*-direction), if it is further stretched in *y*-direction (perpendicular to *x*), the chains turn parallel to *y*. Since not all the molecular chains arranged in *x*-direction can be turned to *y*, there must be some local regions aligned regularly either in *x*- or in *y*-direction. Between such a region and its surroundings, which has not oriented so orderly or other regions arranged in different directions, boundary defects are generated. They lead to the appearance of new types of localized states, and cause the increase of the number of states. When the samples are drawn in three steps (i.e., succesively along *x*-, *y*-, and *x*-directions), the molecular chains initially oriented in *y*-direction would turn parallel to *x*-direction again. In this way, the arrangement of chains tends to be more complex, causing the number of localized states to increase to six.

The observations with electron microscope established that no observable supermolecular structure was formed in our experimental conditions of performing drawing biaxially in sequence or simultaneously in *x*- and *y*-direction[10]. The crystallinity determined from the density gradient measurements is not high. The investigations of FTIR/PAS indicated that the content of trans-isomer of aliphatic segments increases with the rise of $\Delta(xy)z$[2]. Therefore, the reason that the increase of the depth of localized levels arising from the rise of $\Delta(xy)z$ is related to the content of trans-isomer. The higher the content of trans-isomer is, the greater the extent of regular arrangement that molecular

chains along the film plane, and the deeper the localized level formed will be.

For the sample BS-1, drawn simultaneously in x- and y-direction, it can be found from Table 2 that, in spite of the degree of planar orientation is not high, the depth of localized level is large. While in the samples drawn biaxially in sequence, only the rodlike crystalline structure of PET oligomers was observed with electron microscope. As to the samples drawn simultaneously in x- and y-direction, only a net-like structure composed of some very small bright strips ($0.1-0.3\ \mu m$) was revealed. Probably it is this kind of structure that introduces the deeper localized levels. Because of stretching simultaneously in x- and y-direction, and using the same drawing speed and the same degree of enlargement, the chains arrange randomly in two directions. Moreover, since $\Delta(xy)z$ is lower, more kinds of boundary defects cannot be formed. In this way, though the depth of localized level is very large, the number of localized states only increases from two of amorphous to three.

The formation process of supermolecular structure of amorphous PET in isothermal treatment could be divided into two steps[11, 12]. Initially, the small crystalline domains generated in the noncrystalline phase where the molecular chains oriented disorderly (nucleation). Then, the crystalline structure called mosaic block was produced. When the annealing time was not too long, it was mainly the mosaic blocks that appeared continuously from amorphous phase, thereby caused the density and crystallinity to rise. After a time, the number of mosaic blocks increased no more, but did grow and become perfect by reorganizing the amorphous regions, rejecting defects from crystals, and forming more regular folding surfaces. Thus clear boundaries appeared between crystalline and noncrystalline regions.

The wide-angle X-ray diffraction patterns of crystallized PET are shown in Fig. 4. It indicates that the three peaks, with 2θ angle located at 17°, 23.5°, and 26° respectively,

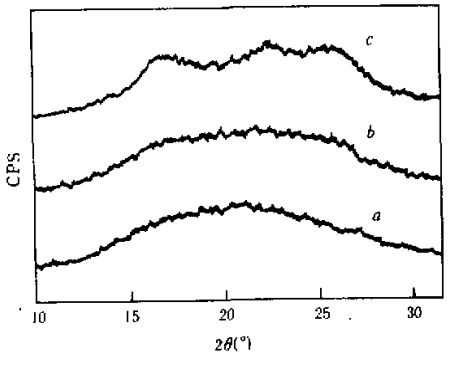

Fig. 4. Wide-angle X-ray diffraction patterns of crystallized PET films. *a*: AMOR; *b*: C-6; *c*: C-8.

become clear gradually with the rise of crystallinity. These peaks are produced by the diffraction of three crystal planes of (010), ($\bar{1}$10) and (100) of PET crystals[13]. The results of X-ray diffraction show that the crystal planes are formed apparently as the crystallinity increases to 20 %.

From the crystallization processes of PET by annealing, we find that when the crystallinity is low, clear crystalline and noncrystalline regions cannot be formed by nucleation. With the rise of X_c and the growth and approaching perfection of mosaic blocks, the boundaries of crystalline and noncrystalline regions emerge gradually, which causes the kinds of structural defects to enlarge, leads the number of localized states to increase. Therefore, the number of these states in specimen C-1 and C-2 is still two, only the depth of localized levels has a little increase as compared with the amorphous sample. As the crystallinity rises further, the number of mosaic blocks increases successively, the structure of mosaic blocks becomes more perfect, thus the boundaries between the crystalline and noncrystalline regions become clear. At the same time, the boundaries among the crystalline regions arranged in different directions probably appear. This is to say, the increase of crystallinity brings about the rise of the types of structural defects, corresponding to the increase of the kinds and the number of localized states. In the case of C-3 and C-4, this number increases to three. When crystallinity is about 20 %(C-5), four localized states appear. After that, when X_c increases continuously, crystallization is in a stage of perfection, the boundaries among the crystalline and noncrystalline regions are more clear, but the kinds of localized states originated from the boundary defects do not increase significantly, therefore, even for sample C-8 with a higher crystallinity, only the depth of localized levels rises, while the number of these states increases no more.

It is suggested, according to the structure variations during the crystallization processes that the stage *a* and stage *b* in Fig. 3 correspond to the two processes of crystallization respectively. The fast rise of the depth of localized levels is caused by the increase of the crystalline domains in amorphous phase; the growth and perfection of the domains give little effects on the depth of localized levels.

In regard to γ-irradiated samples, from Table 2 we can find that the number of localized states is always three until irradiation dose increases to 3 MGy. Four localized states appear when irradiation dose rises to 4 MGy. The study of wide-angle X-ray diffraction and FTIR/PAS indicated that there were not any clear crystalline region formed and no variation of chain conformation revealed in the samples. Therefore, the number of localized states of γ-irradiated PET increases from two of amorphous to four is not caused by the rise of the kinds of structural defects arisen from new boundaries among the crystalline and noncrystalline regions.

The results of FTIR/PAS and absorption spectra of ultraviolet and visible light for γ-irradiated PET are shown in Fig. 5. The bands within the range of $1500-1580\ cm^{-1}$ relate to the stretching vibration of phenyl C=C of chains. When PET is irradiated by γ-rays with large dose, the free radical 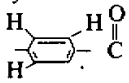 is generated[14]. As this radical

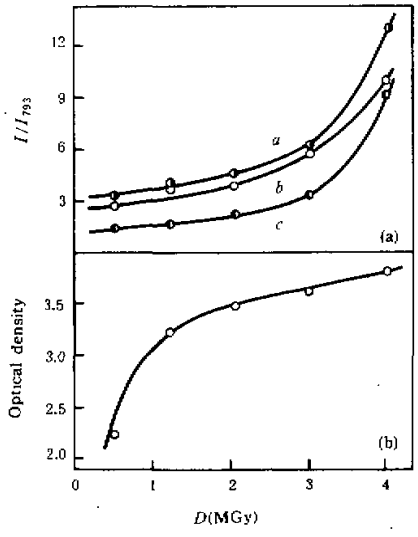

Fig. 5. Correlation of the intensity of stretching vibration band of phenyl C=C and the maximum optical density with irradiation dose for γ-irradiated PET films. *a*: I_{1505}/I_{793}; *b*: I_{1574}/I_{793}; *c*: I_{1519}/I_{793}.

combines with O_2 in the air, group 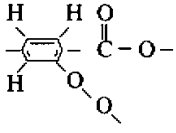 (3) is formed, which results in

the variation of $\nu_{c=c}$ vibration of phenyl. The variation leads to the changes of band intensity in the range of $1510\pm8\,cm^{-1}$ and $1577\pm8\,cm^{-1}$ [15]. The evident enhancement of intensity of photoacoustic signal of bands 1505, 1519 and 1574 cm^{-1} in Fig. 5 (a) suggests that the concentration of group (3) increases as irradiation dose rises. Moreover, the increase of the intensity of maximum optical density of ultraviolet and visible light, as shown in Fig. 5(b), also indicates that the density of group (3) in γ-irradiated samples increases with the rise of irradiation dose.

The important characteristics of γ-irradiation effects are the cross-linking or degradation of molecular chains. Within the dose range used in our experiments, no gel has been found in γ-irradiated PET samples. It can be found from Table 1 that the polymer chains are broken, average molecular weight decreases gradually as the irradiation dose rises. According to the measurements of dispersion degree, the molecular weight distribution becomes more and more broad with the increase of irradiation dose. In consequence, the effects of large dose γ-irradiation are: (1) the molecular chains of PET are broken, average molecular weight decreases, and (2) the group density of phenyl with oxy-

gen substituent in the chains increases. These structural variations give rise to the production of structural defects at the breaking points of molecular chains and the places of groups of phenyl with oxygen as well as the places where matter with low molecular weight generates, which leads to the appearance of new kinds of localized states, the increase of the number of these states and the depth of localized levels.

IV. CONCLUSIONS

After amorphous PET is drawn biaxially, crystallized by annealing and irradiated with large dose γ-rays respectively, because of the structure changes of molecular orientation, crystalline and composition of chains, the structural defects of boundary are generated at the boundaries among the oriented and nonoriented regions, the two oriented regions, the crystalline and noncrystalline regions or the two crystalline ones. Furthermore, the structural defects caused by breaking of polymer chains and the group (3) are also produced. As the kinds of defects rise, the number of localized states increases from two to six, the distribution of localized levels tends to be more complicated, which not only leads to the increase of the mean depth of localized levels, but also the broadening of depth distribution.

REFERENCES

[1] D. A. Seanor, Electrical Properties of Polymers (Academic Press, New York, 1982), p. 21.
[2] Y. Zhou, J. Zhang, X. Zhang and J. Yang, *Makromol. Chem.*, **189**(1988), 2153.
[3] R. J. Samuels, *J. Appl. Polym. Sci.*, **26**(1981), 1383.
[4] S. Hu and M. Xu, *Huaxue Tongbao*, (3) (1985), 20(in Chinese).
[5] X. Zhang, Y. Zhou and J. Zhang, in "Proceedings of the 7th International Symposium on Electrets, 1991", edited by R. Gerhard-Multhaupt, W. Kunstler, L. Brehmer and R. Danz (IEEE Inc., Berlin, 1991), p. 618.
[6] J. Turnhout, Thermally Stimulated Discharge of Polymer Electrets (Elsevier, Amsterdam, 1975), p. 61.
[7] J. Yu, S. Liu and R. Qian, *Polym. Commun.*, (4) (1985), 282(in Chinese).
[8] J. Turnhout, Electrets, edited by G. M. Sessler (Springer-Verlag, Berlin, 1980), pp. 99, 54.
[9] J. G. Simmons and G. W. Taylor, *Phys. Rev.*, **B5**(1972), 1619.
[10] L. Zhu, Q. Yang, Z. Wen, J. Guan, M. Xu and R. Qian, *Polym. Commun.*, (4)(1983), 310 (in Chinese).
[11] S. Fakirov, E. W. Fischer, R. Hoffmann and G. F. Schmidt, *Polymer*, **18**(1977), 1121.
[12] G. C. Alfonso, E. Pedemonte and L. Ponzetti, *Polymer*, **20**(1979), 104.
[13] N. T. Wakelyn, *J. Appl. Polym. Sci.*, **28**(1983), 3599.
[14] D. T. Turner, The Radiation Chemistry of Macromolecules (Vol. 2), edited by M. Dole (Academic Press, New York, 1973), p. 137.
[15] Z. Wang, X. He and D. Sun, Applied Infra-red Spectroscopy (Petroleum Industry Press, Beijing, 1982), p. 170 (in Chinese).